International Journal of Naval Architecture and Ocean Engineering 11 (2019) 970–979

Contents lists available at ScienceDirect

International Journal of Naval Architecture and Ocean Engineering

journal homepage: http://www.journals.elsevier.com/international-journal-of-naval-architecture-and-ocean-engineering/

Static performance analysis of deepwater compliant vertical access risers

Min Lou [a, *], Run Li [a], Wugang Wu [b], Zhengshou Chen [c]

[a] College of Petroleum Engineering, China University of Petroleum, China
[b] Kunming Shipborne Equipment Research and Test Center, China Shipbuilding Industry Corporation, Kunming 650051, China
[c] State Key Laboratory of Coastal and Offshore Engineering, Dalian University of Technology, China

ARTICLE INFO

Article history:
Received 20 November 2018
Received in revised form
9 April 2019
Accepted 29 April 2019
Available online 18 May 2019

Keywords:
Compliant vertical access riser
Geometrical nonlinearity
Static analysis

ABSTRACT

Compliant Vertical Access Risers (CVARs) are compliant systems that incorporate a differentiated geometric configuration that allows the exploitation of oil and gas in deepwater fields and enables a number of operational advantages in the offshore system. One of the main features of CVAR systems is that they allow direct intervention procedures to be applied to the well bore, enabling workover operations to be performed directly from the production platform. Based on the principles of virtual work and variation, a static geometric nonlinear equation of CVARs is derived and applied in this study. The results of this study show that the two ends of the riser as well as the transition region are subject to high stress, while the positions of the floating platform exert significant effects on the geometry of the riser configuration. Compliance and buoyancy factors should be set moderately to reduce the CVAR stress. In addition, the buoyancy modules should be placed in the lower region, in order to maximize the operation advantages of CVAR.

1. Introduction

Over the last few decades, a number of risers have been developed for use in different marine environments in order to meet the requirements of offshore oil exploration and development. Indeed, as hydrocarbon exploitation moves into ever deeper waters, riser forms are continually and rapidly innovated. Four main types are currently employed on deepwater platforms (Wang et al., 2009.), top tension (TTR), steel catenary (SCR), flexible (FR), and hybrid (HR) risers.

One of the main disadvantages of TTRs is their poor compliance (Howells, 1996), while SCRs are subject to serious fatigue problems, especially in the touchdown zone (Claudio et al., 2004.). Similarly, due to their special material nature, FRs are not suitable for use in high temperature and pressure fields (Martins and Higashi, 2000), while the production costs of large diameter flexible risers are so prohibitive that their development space remains minimal (Zhang et al., 2010.). In addition, the connective joints of HR are complex and problematic to use with an anchor system (Elosta et al., 2013.).

Compliant Vertical Access Risers (CVARs) are systems that incorporate a differentiated geometric configuration to enable the exploitation of oil and gas in deepwater fields. These systems provide a number of operational advantages in offshore situations (Fig. 1). The upper region riser length is fitted with strakes or fairings to suppress riser Vortex Induced Vibrations (VIVs) and a heavy weight coating (or alternative clump weight) is applied to part of the length. In the transitional region, the buoyancy modules are fitted. The riser sections in the lower region are also fitted with large diameter buoyancy modules near its top. One of the key features of CVAR systems is that they allow direct intervention procedures within the well bore, enabling workover operations to be performed directly from the production platform. This characteristic eliminates the necessity of hiring specific units for these tasks, and means that this new riser system is economically attractive. These systems therefore have the potential to reduce completion and well intervention costs (Chris et al., 2004; Kuroiwa and Nishigaki, 2002.).

Compared with TTRs, SCRs, and FRs, less research has been carried out on CVARs. Mungall and Haverty (2004) proposed the concept of a semi-submersible platform combined with a CVAR for deployment in the Gulf of Mexico, this study was restricted to

* Corresponding author.
E-mail addresses: shidaloumin@163.com (M. Lou), 1393523066@qq.com (R. Li), 1195681687@qq.com (W. Wu), 15764257302@163.com (Z. Chen).
Peer review under responsibility of Society of Naval Architects of Korea.

https://doi.org/10.1016/j.ijnaoe.2019.04.007

Nomenclature

α	*The curved shape of the riser*
r	Positional vector
u	Static displacement of one point on the riser
s	Arc length
K	Curvature
ds	Infinitesimal
δU_a	*Variation in axial strain energy*
δU_b	*Variation in bending strain energy*
T_e	*Effective tension*
T	*Actual tension*
v	Poisson's ratio
P_e	*External pressure*
P_i	*Internal pressure*
A_e	*Cross-sectional area outside the riser*
A_i	*Cross-sectional area inside the riser*
δW_e	*Virtual work of effective gravity*
δW_f	*Virtual work done by loads*
δW_C	*Virtual work done by current*
ρ_r	*Density of the riser*
ρ_e	*Density of seawater*
ρ_i	*Density of internal fluid*
g	Acceleration due to gravity
C_{Dt}	*Coefficient of tangential drag*
C_{Dn}	*Coefficient of normal drag*
ε	Axial strain
m_r	*Weight of riser*
m_i	*Weight of internal fluid*
EA	Axial tensile stiffness

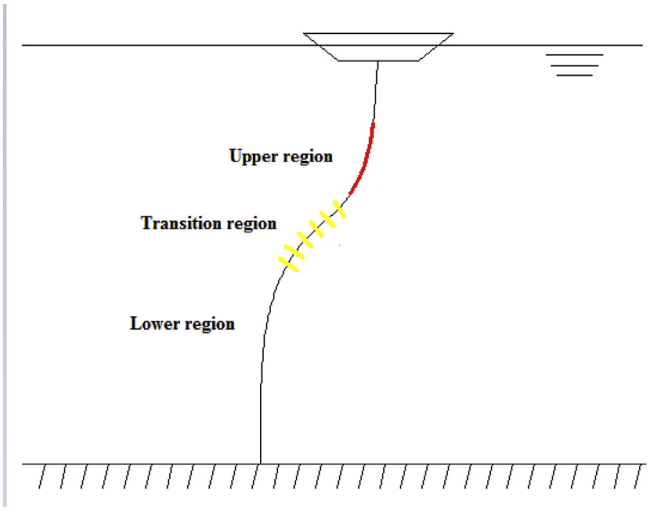

Fig. 1. Conceptual diagram of a CVAR.

applications below 2,400 m. Similarly, Kuroiwa and Nishigaki (2002) proposed the use of a unique Floating Production Storage and Offloading (FPSO) design, a CVAR-FPSO, and studied the interactions between this riser system and associated tubing, while Martins (2013) optimized this design by incorporating the NSGA-II (the Elitist Nondominated Sorting Genetic Algorithm) and DOE (Design of Experiments) methods, respectively. Zhen and Yang et al. (2010) also adopted the DOE designed method to establish an approximate model, providing a simple weight optimization for a CVAR system.

At present, the research on CVARs are mainly in the conceptual design stage, and there is no detailed elaboration on the mechanical models of CVAR. To address this, in this paper, based on virtual work and variational principles, a static geometric nonlinear equation of CVARs is derived, and then static properties of CVARs are discussed.

2. The CVAR equilibrium equation

The model applied in this paper is based on virtual work and variational principles. Strain energy in this expression is mainly produced by axial deformation and bending deformation, while the main virtual work of external loads include effective gravity, buoyancy, and current (Yang and Xiao, 2014.).

2.1. Static equilibrium and deformation

Relative to its external diameter, the length of the CVAR is much longer and has a large slenderness ratio. Therefore, a CVAR is usually considered as a three-dimensional (3-D) rod-like element rather than a cylindrical shell-like element. The center-line position of the CVAR can therefore be described using a 3-D orthogonal coordinate system (Fig. 2). Two motion states for the riser are defined in this study, the first of which is the ideal or undeformed state. The position of the vertical riser is expressed by the position vector $\boldsymbol{r}_0$, as follows:

$$\boldsymbol{r}_0(\alpha) = x_0(\alpha)i + y_0(\alpha)j + z_0(\alpha)k \tag{1}$$

The parameter α is a scalar, used to define the curved shape of the riser.

The second riser state is static balance. In this case, the point coordinates on riser curves are represented by the positional vector $\boldsymbol{r_s}$, as follows:

$$\boldsymbol{r_s}(\alpha) = \boldsymbol{r}_0(\alpha) + \boldsymbol{u_s}(\alpha) = x_s(\alpha)\boldsymbol{i} + y_s(\alpha)\boldsymbol{j} + z_s(\alpha)\boldsymbol{k} \tag{2}$$

The vector $\boldsymbol{u_s}$ represents the static displacement of one point on

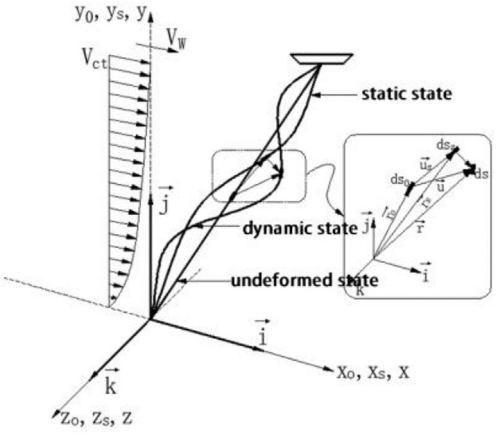

Fig. 2. The three configurations of a 3-D marine riser.

the riser:

$$\boldsymbol{u}_s(\alpha) = u_s(\alpha)\boldsymbol{i} + v_s(\alpha)\boldsymbol{j} + w_s(\alpha)\boldsymbol{k} \tag{3}$$

In this expression, arc length in an undeformed state, the arc length in a static balance state:

$$s'_0 = \sqrt{x'^2_0 + y'^2_0 + z'^2_0} \tag{4}$$

and;

$$s'_s = \sqrt{x'^2_s + y'^2_s + z'^2_s} = \sqrt{(x'_0 + u'_s)^2 + (y'_0 + v'_s)^2 + (z'_0 + w'_s)^2} \tag{5}$$

In this expression, the superscript (') represents the partial derivative of the independent variable α.

Thus, the curvature K of the 3-D riser is expressed as (Zhang, 2002.):

$$K = \frac{d\theta}{ds} = \frac{1}{s'^3_s}\sqrt{(x''_s y'_s - x'_s y''_s)^2 + (y''_s z'_s - y'_s z''_s)^2 + (x''_s z'_s - x'_s z''_s)^2} \tag{6}$$

2.2. Virtual work equation

In this part, the axial and bending deformation of risers is considered when developing the virtual work principle.

2.2.1. Axial strain energy

Axial CVAR deformation is caused by two factors, one is the actual riser tension while the other is the pressure difference between inner and outer fluid. Thus, the variation in axial strain energy of the infinitesimal ds is as follows:

$$\delta U_a = \int_{\alpha_0}^{\alpha_t} T_e \delta s' d\alpha = \int_{\alpha_0}^{\alpha_t} T_e \left[\left(\frac{x'}{s'}\right)\delta u' + \left(\frac{y'}{s'}\right)\delta v' + \left(\frac{z'}{s'}\right)\delta w'\right] d\alpha \tag{7}$$

And the effective tension T_e is as follows (Chucheepsakul et al., 2003):

$$T_e = T + 2v(P_e A_e - P_i A_i) \tag{8}$$

T is the actual tension of the riser, v is the Poisson's ratio of the riser material, P_e is the external pressure, P_i is the internal pressure, A_e is the cross-sectional area outside the riser, and A_i is the cross-sectional area inside the riser.

2.2.2. Bending strain energy

Variation in bending strain energy is expressed as follows, which is derived from Eq. (9):

$$\theta' = s'\kappa = \frac{1}{s'^2}\sqrt{(x''y' - x'y'')^2 + (y''z' - y'z'')^2 + (x''z' - x'z'')^2} \tag{9}$$

Substituting $s's'' = x'x'' + y'y'' + z'z''$, variation in bending strain energy can be expressed as follows:

$$\begin{aligned}\delta U_b = &\int_{\alpha_0}^{\alpha_t}\left\{\left[\frac{B}{s'^2}\frac{\partial}{\partial\alpha}\left(\frac{x'}{s'}\right)\right]\delta u'' - \left[\frac{s''}{s'^3}\frac{\partial}{\partial\alpha}\left(\frac{x'}{s'}\right) + \frac{\kappa^2 x'}{s'}\right]\delta u'\right\}d\alpha \\ &+ \int_{\alpha_0}^{\alpha_t}\left\{\left[\frac{B}{s'^2}\frac{\partial}{\partial\alpha}\left(\frac{y'}{s'}\right)\right]\delta v'' - \left[\frac{s''}{s'^3}\frac{\partial}{\partial\alpha}\left(\frac{y'}{s'}\right) + \frac{\kappa^2 y'}{s'}\right]\delta v'\right\}d\alpha \\ &+ \int_{\alpha_0}^{\alpha_t}\left\{\left[\frac{B}{s'^2}\frac{\partial}{\partial\alpha}\left(\frac{z'}{s'}\right)\right]\delta w'' - \left[\frac{s''}{s'^3}\frac{\partial}{\partial\alpha}\left(\frac{z'}{s'}\right) + \frac{\kappa^2 z'}{s'}\right]\delta w'\right\}d\alpha\end{aligned} \tag{10}$$

2.2.3. Virtual work of external force

Our workflow in this respect is as follows (Monprapussron et al, 2004.).

(1) Effective gravity

The virtual work of effective gravity is as follows:

$$\delta W_e = -\int_{\alpha_0}^{\alpha_t}(\rho_r A_r - \rho_e A_e + \rho_i A_i) g s' \delta v d\alpha \tag{11}$$

Where ρ_r, ρ_e, ρ_i are densities of the riser, seawater and internal fluid, respectively. A_r, A_e, A_i are the areas of the riser cross section, outer riser cross section and the inner riser cross section, respectively. And g is the acceleration due to gravity.、

(2) Load of the buoyancy modules and heavy coating

Buoyancy modules and heavy coatings are distributed in different regions along the CVAR, and the virtual work done by their respective loads are:

$$\delta W_f = -\int_{\alpha_0}^{\alpha_t} f s' \delta v d\alpha \tag{12}$$

A force, f, is produced by the buoyancy modules and heavy coating, which is in the vertical direction.

(3) Current load

If we decompose the current velocity into the normal and tangential directions, the virtual work done by the current is:

$$\begin{aligned}\delta W_c = &\left(\frac{x'}{s'}\frac{1}{2}C_{Dt}\rho_e u_{ct}^2 + \frac{y'}{s'}\frac{1}{2}C_{Dn}\rho_e u_{cn}^2\right)\delta u d\alpha \\ &+ \left(\frac{y'}{s'}\frac{1}{2}C_{Dt}\rho_e u_{ct}^2 - \frac{x'}{s'}\frac{1}{2}C_{Dn}\rho_e u_{cn}^2\right)\delta v d\alpha\end{aligned} \tag{13}$$

2.3. Constraint equation

Because of the presence of the unknown item T_e, another constraint equation is necessary. In this case, we tested the hypothesis that the total length of riser is constant. To do this, the CVAR was allowed to elongate while holding total length almost constant, using the following constraint equation:

$$\boldsymbol{r}'\boldsymbol{r}' = (1+\varepsilon)^2 = \left(1+\frac{T}{EA}\right)^2 \tag{14}$$

In this expression, EA refers to the axial tensile stiffness of the CVAR. In cases where the axial strain was small, the higher-order item was omitted, as follows:

$$\frac{1}{2}(\boldsymbol{r}'\boldsymbol{r}'-1) = \frac{T_e - 2\nu\rho_e A_e}{EA} \tag{15}$$

2.4. A CVAR mechanical model

According to the virtual work principle, deformation energy generated by the virtual work of internal force is equal to the sum of the external force, as follows:

$$\delta\pi = \delta U_a + \delta U_b - \delta W_c - \delta W_e - \delta W_f \tag{16}$$

All loads in the virtual work equation act in the XOY plane (Fig. 2). In the equilibrium configuration, $\delta u = \delta x, \delta v = \delta y$, so the mechanical model is simplified as:

$$\begin{aligned}\delta\pi = &\int_{\alpha_0}^{\alpha_t}\left\{\left[\lambda\left(\frac{x'}{s'}\right) - EI\frac{s''}{s'^3}\frac{\partial}{\partial\alpha}\left(\frac{x'}{s'}\right)\right]\delta x' + \left[\lambda\left(\frac{y'}{s'}\right) - EI\frac{s''}{s'^3}\frac{\partial}{\partial\alpha}\left(\frac{y'}{s'}\right)\right]\delta y'\right\}d\alpha \\ &+ \int_{\alpha_0}^{\alpha_t}\left\{\left[\frac{EI}{s'^2}\frac{\partial}{\partial\alpha}\left(\frac{x'}{s'}\right)\right]\delta x'' + \left[\frac{EI}{s'^2}\frac{\partial}{\partial\alpha}\left(\frac{y'}{s'}\right)\right]\delta y''\right\}d\alpha - \int_{\alpha_0}^{\alpha_t}\left(F_x\delta x + F_y\delta y s'\right)d\alpha\end{aligned} \tag{17}$$

Where $\lambda = T_e - EI\kappa^2$. Next:

$$F_x = \frac{x'}{2s'}C_{Dt}\rho_w u_{ct}^2 + \frac{y'}{2s'}C_{Dn}\rho_w u_{cn}^2$$

$$F_y = \frac{y'}{2s'}C_{Dt}\rho_w u_{ct}^2 - \frac{x'}{2s'}C_{Dn}\rho_w u_{cn}^2 - (\rho_r A_r - \rho_e A_e + \rho_i A_i)g + f$$

The constraint equation for the elongation condition is:

$$\int_{\alpha_0}^{\alpha_t}\left[\frac{1}{2}\left(x'^2 + y'^2 - 1\right) - \frac{\lambda - 2\nu(\rho_e A_e - \rho_i A_i) + m_i U_i^2}{EA}\right]d\alpha = 0 \tag{18}$$

3. Solving method and model verification

3.1. Finite Element (FE) discretization

The Galerkin method was applied to discretize the static mechanics equation of the CVAR. The geometric configuration of a CVAR is special and its solution process is unpredictable; moreover its configuration may become U-shape or C-shape. If the units are divided along x (horizontal direction) or y (vertical direction), it cannot be solved. To do this, units along the length were divided and s was taken as an independent variable. Then cubic Hermit interpolation was applied, using the effective tension for linear interpolation. Thus, $[N]$, [p] are the shape functions of the cubic Hermit interpolation and linear interpolations, respectively, which are guided by the specific expressions:

$$\left.\begin{aligned} N1 &= 1 - 3\frac{s^2}{Le^2} + 2\frac{s^3}{Le^3} \\ N2 &= s - 2\frac{s^2}{Le} + \frac{s^3}{Le^2} \\ N3 &= 3\frac{s^2}{Le^2} - 2\frac{s^3}{Le^3} \\ N4 &= \frac{s^2}{Le} + \frac{s^3}{Le^2} \end{aligned}\right\} \tag{19}$$

and;

$$\left.\begin{aligned} p1 &= 1 - \frac{s}{Le} \\ p2 &= \frac{s}{Le} \end{aligned}\right\},\ [P] = [P_1\ P_2] \tag{20}$$

The interpolation expression of displacement and effective tension are as follows:

$$\begin{aligned}\boldsymbol{r} = \begin{Bmatrix} \mathrm{r}_1 \\ \mathrm{r}_2 \end{Bmatrix} &= \begin{bmatrix} N_1 & N_2 & 0 & 0 & N_3 & N_4 & 0 & 0 \\ 0 & 0 & N_1 & N_2 & 0 & 0 & N_3 & N_4 \end{bmatrix}\begin{Bmatrix} U_{x_1} \\ U_{x'_1} \\ U_{y_1} \\ U_{y'_1} \\ U_{x_2} \\ U_{x'_2} \\ U_{y_2} \\ U_{y'_2} \end{Bmatrix} \\ &= [N]\{U\} = [N]\boldsymbol{U}\end{aligned} \tag{21}$$

and;

$$\boldsymbol{\lambda} = [\mathrm{p}]\{\lambda\} = [\mathrm{p}_1\ \ \mathrm{p}_2]\begin{Bmatrix} \lambda_1 \\ \lambda_2 \end{Bmatrix} \tag{22}$$

Thus, $\delta\pi = 0$, the variational principle is as follows:

$$\boldsymbol{R} = \int_0^s EI\left[N''\right]^T\left[N''\right]ds\boldsymbol{U} + \int_0^s [p]\{\lambda\}[N']^T[N']ds\boldsymbol{U} - \int_0^s [N]^T\boldsymbol{f}ds\boldsymbol{U} = 0 \tag{23}$$

This is then transformed into a matrix form, as follows:

$$\{R\} = ([K1] + [p]\{\lambda\}[K2])\{U\} - \{F1\} = 0 \tag{24}$$

Therefore, $[K1] = \int_0^L [N'']^T EI[N'']ds$, $[K2] = \int_0^L [N']^T[N']ds$, $\{F1\} = \int_0^L [N]^T\boldsymbol{f}ds$ and the hydrostatic pressure is same as the effective tension. This enables us to use linear interpolation, as

follows:

$$P_e = [P]\{P_e\} \tag{25}$$

Eq. (18) was discretized by multiplying both sides by $\delta\lambda$and then the units were integrated, as: units, as follows:

$$\{\boldsymbol{G}\} = \int_0^L [P]^T \left\{ \frac{1}{2}\left(\{U\}^T[N']^T[N']\{U\} - 1\right) - \frac{1}{EA}[P]\left[\{\lambda\} - 2v\{P_e\}A_e + m_i U_i^2\right]\right\}\delta\lambda ds \tag{26}$$

The variational principle is therefore as follows:

$$\{G\} = \frac{1}{2}[K3]\{U\} + [K4]\{\lambda\} + \{F2\} \tag{27}$$

Thus, $[K3] = \int_0^L [P]^T\{U\}[N']^T[N']ds$, $[K4] = -\frac{1}{EA}\int_0^L [P]^T[P]ds$, and

$$\{F2\} = \frac{2v}{EA}\int_0^L [P]^T[P]\{P_e\}Aeds - \int_0^L \frac{1}{2}[P]^T ds.$$

Because the expressions {R}{G} are Taylor extended, the following high order term was omitted:

$$\begin{aligned}\{R\}^{n+1} &= \{R\}^n + \frac{\partial R}{\partial U}\{\Delta U\} + \frac{\partial R}{\partial \lambda}\{\Delta\lambda\} \\ &= \{R\}^n + [K2]\{U\}[P]\{\Delta\lambda\} \\ &+ ([K1] + [P]\{\lambda\}[K2])\{\Delta U\}\end{aligned} \tag{28}$$

and;

$$\begin{aligned}\{G\}^{n+1} &= \{G\}^n + \frac{\partial G}{\partial U}\{\Delta U\} + \frac{\partial G}{\partial \lambda}\{\Delta\lambda\} \\ &= \{G\}^n + [K3]\{\Delta U\} + [K4]\{\Delta\lambda\}\end{aligned} \tag{29}$$

Then the general matrix equations were synthesized, as follows:

$$\begin{bmatrix} [K1] + [P]\{\lambda\}[K2] & [K2]\{U\}[P] \\ [K3] & [K4] \end{bmatrix}\begin{Bmatrix} \Delta U \\ \Delta\lambda \end{Bmatrix} = -\begin{Bmatrix} R \\ G \end{Bmatrix} \tag{30}$$

The incremental form equation is as follows:

$$[K]\{\Delta y\} = \{F\} \tag{31}$$

Thus, Eq. (31) is the CVAR static analysis equation, while the static matrix equation of the CVAR is a typical non-linear example. However, it is necessary to iterate this expression to obtain the geometrical configuration and effective tension at the equilibrium position.

3.2. Comparative results

On the basis of our input parameters MATLAB was used to design a reasonable storage structure and to calculate FEs. The MATLAB software was used to calculate the static configuration, effective tension, and bending moment distribution of the SCR (Figs. 3 and 4). The results calculated using this FE approach are similar to those already present in the literature (Chen, 2011), they have the same configuration, and all show that the effective top tension of the far-end is about 1,030 kN, while the largest bending moment of the near-end is near 775 kNm. These measurements also reveal that the highest point of the buoyancy module riser occurs about 740 m from the bottom of the pipe. Thus, the FE program designed and used in this study is both correct and effective, and can be applied to analyze the non-linear static CVAR mechanics.

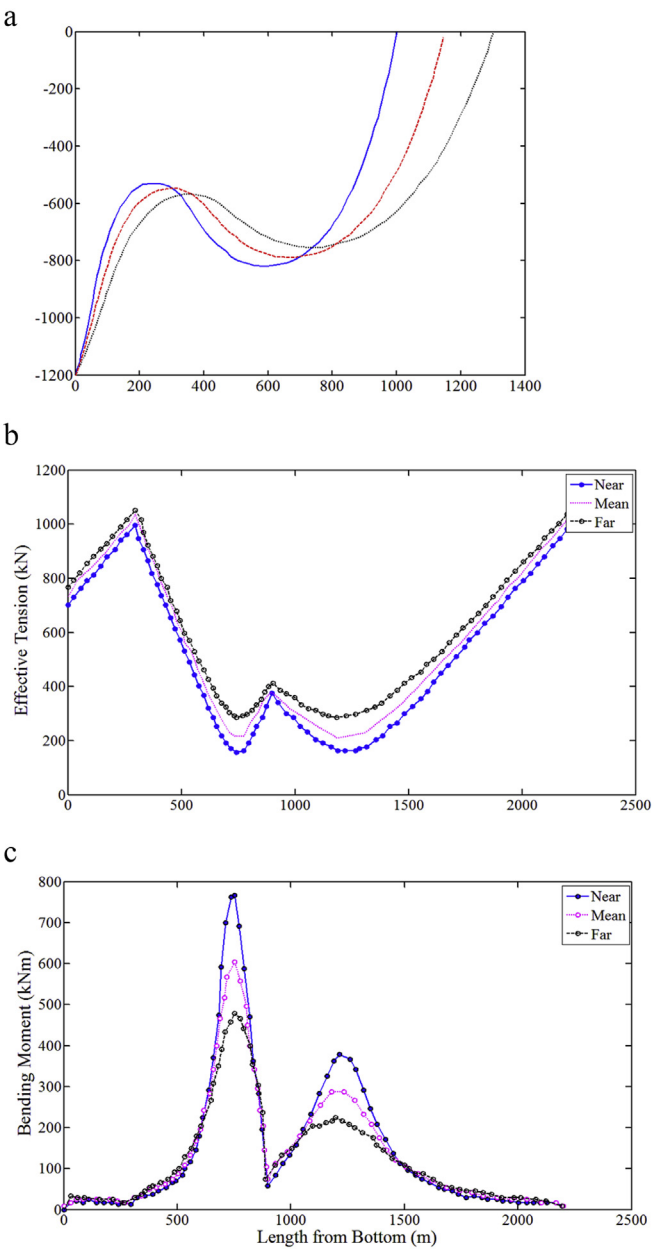

Fig. 3. Chen's results. (a) Equilibrium configuration. (b) Effective tension force along the bottom of riser. (c) Moment along the bottom of the riser.

4. Mechanical performance analysis

4.1. Parameter setting

In this part of our analysis, the far-end (i.e. Far, xL = 760 m) was defined as drift away from the wellhead (Fig. 5), while the intermediate position was set as the equilibrium position (i.e. Equilibrium, xL = 610 m), and the near-end was defined as the position when offset was closest to the wellhead (i.e. Near, xL = 460 m). Thus, assuming that the offset of the floating body is 150 m in extreme sea conditions, a water depth of 2,400 m was applied as an example and a static mechanical CVAR analysis was performed at

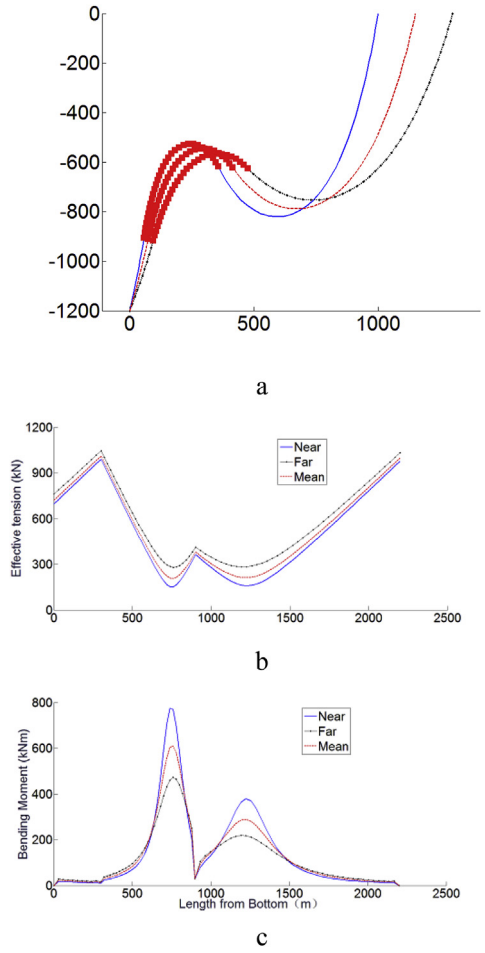

Fig. 4. The results presented in this study. (a) Equilibrium configuration. (b) Effective tension force along the bottom of riser. (c) Moment along the bottom of the riser.

three locations. The design parameters are listed in Table 1.

Both ends of the riser are solid-joint. Extreme sea conditions were considered, i.e. the 100 year return period loop current (surface current = 2.71 m/s, vessel offset = 100m). The vessel offset was considered in the position analysis (near end, equilibrium position, and at the far end), and the result is shown in Section 4.2.

Table 1
Parameters used in the CVAR static model.

Detailed parameters	Value
Horizontal distance between the wellhead and the platform X(m)	610
Water depth Z (m)	2,438
Total length of the riser S (m)	2,601
Upper region length L_u(m)	1,695
Transitional region length L_t(m)	416
Lower region length L_1(m)	490
Length of the buoyancy module in the lower region L_{lp}(m)	190
Buoyancy factor of the buoyancy module in the lower region C_{f1}	6
Buoyancy factor of the buoyancy module in the transitional region C_{f2}	2
Buoyancy factor of the buoyancy module in the upper region C_{f3}	−1.5
Location of buoyancy module (from wellhead) (m)	491 to 907
Surging D_x(m)	0
Heaving D_z(m)	0
Outer diameter of the riser D_e(m)	0.3
Thickness of the riser t (m)	0.03
Elastic modulus E (Pa)	$2.07e^{11}$
Poisson's ratio	0.3
Yield strength σ_r	720
Riser material density ρ_r(kg/m^3)	7,850
Seawater density ρ_e(kg/m^3)	1,025
Velocity of sea surface V_{e0}(m/s)	1.72
Normal drag force coefficient C_{Dn}	0.7
Tangential drag force coefficient C_{Dt}	0.03
Gravitational acceleration g (m/s^2)	9.807

4.2. Position analysis

The static configuration and force conditions at the near end, equilibrium position, and at the far end are shown in Fig. 6. As shown in Fig. 6a, the static CVAR configuration changes a great deal due to extreme drift, while, it is clear that the effective tension of both ends is larger than the transition regional (Fig. 6b). If the three positions are compared, the farther away the platform is located, the faster the top tension will increase. Fig. 6(c and d) show that maximum stress occurs in the transitional region and at the bottom where the bending moment is maximal. When the riser is located at the near-end, because of the large CVAR length, the curvature radius of the transitional zone of the buoyancy block sharply becomes smaller, so both the bending moment and stress are at the highest lever, 802 kNm and 508 Mpa, respectively. When the riser is located at the far-end, the transitional region becomes gentle and the bending moment decreases drastically. However, because the bottom end of the riser is connected to the wellhead via a stress joint, excessive offset results in a sharp increase of the bottom bending stress at the bottom of the riser, and reaches a maximum

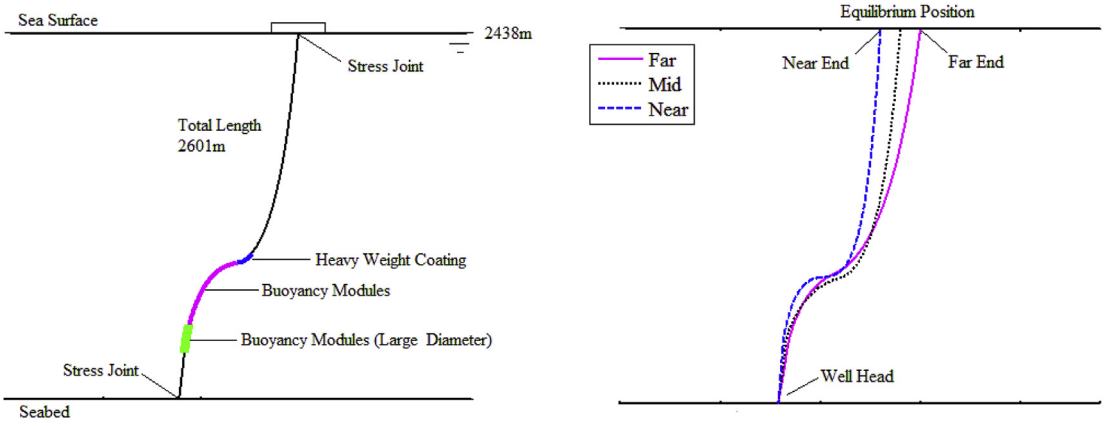

Fig. 5. CVAR configuration.

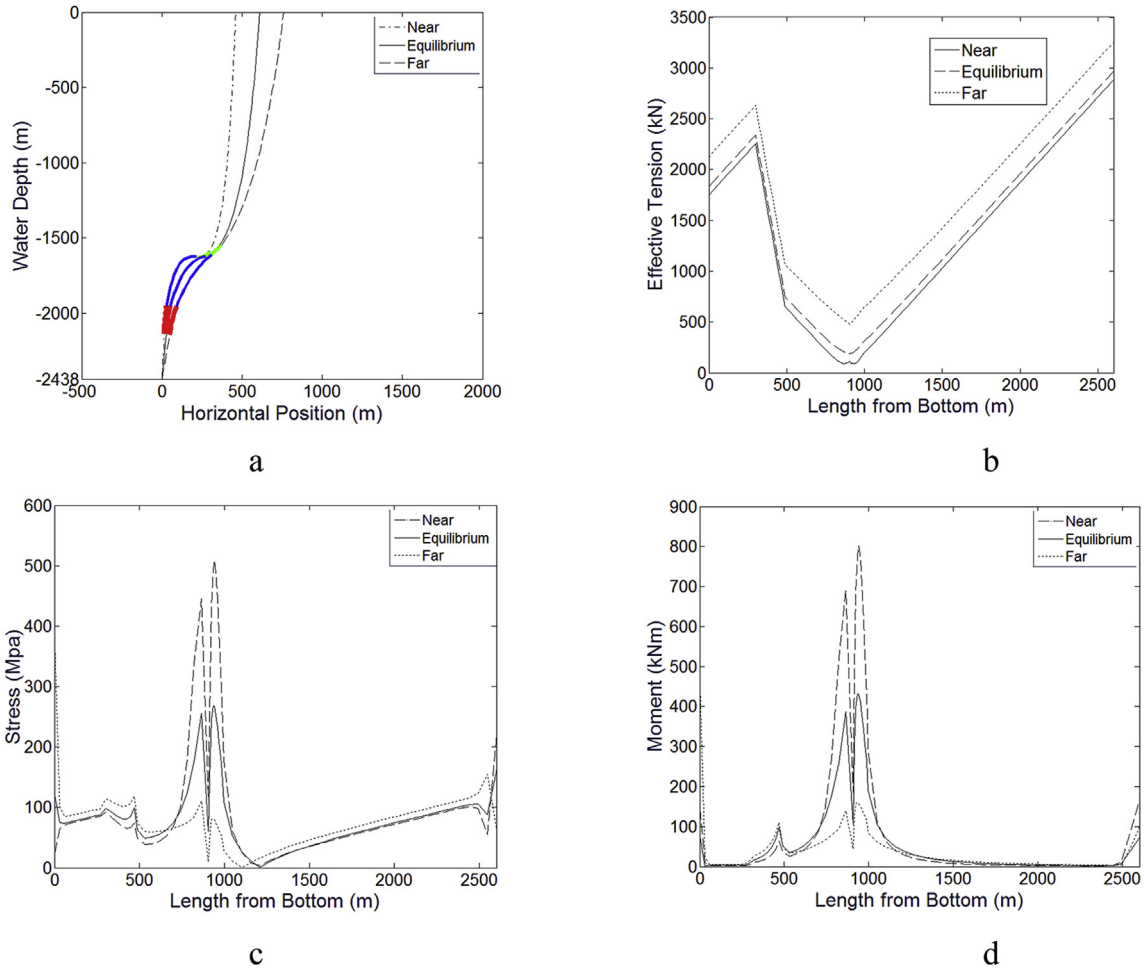

Fig. 6. Static configuration and riser force without current (a) Equilibrium configuration. (b) Effective tension force distribution. (c) Stress distribution. (d) Moment contour.

stress of 373 Mpa.

4.3. Compliance analysis

Compliance is a critical parameter in CVAR design, measured by degrees of compliance (i.e. the ratio between the overlength and the horizontal distance between the suspension point and the wellhead). The overlength is the difference between the total length of the riser and the straight-line distance between the suspension point and the wellhead. Assuming that the overlength of the riser is between 55 m and 175m, corresponding degrees of compliance and associated mechanical properties are listed in Table 2.

Table 2
The influence of degree of compliance.

Overlength/ (m)	Degree of compliance	Max stress/ (Mpa)		
		Nearend	Equilibrium	Far end
55	0.0902	400.5	180.8	591.4
75	0.1230	470.5	230.1	432.8
95	0.1557	527.7	287.3	346.4
115	0.1885	572.7	338.8	289.6
135	0.2213	605.7	381.8	248.8
155	0.2541	640	416.5	233
175	0.2869	644.7	444.3	267.7

The maximum stress and bottom tension curves for CVARs at different degrees of compliance are shown in Fig. 7. These data show that when the CVAR is in different locations, the influence of degree of compliance will be different. When the CVAR is in equilibrium and near-end positions, as compliance increases, so does maximum stress. However, when the riser moves close to the far-end, as compliance increases, maximum stress sharply decreases. Results also show that when the degree of compliance is larger than a given value (0.254 in this model), the maximum CVAR stress increases. Thus, the riser compliance cannot be set too big or too small. If the compliance is too small, when CVAR is in the far-end position, the tension of the riser is at a high level because of the excessive drift and the larger elongation of the rise. However, if the compliance is too big, when CVAR is in the near and equilibrium position, because the riser is too long, the bending moment in the transition zone of buoyancy block is also too large, and the stress caused by bending deformation of riser will soon exceed the allowable stress of stress.

4.4. Buoyancy module analysis

The CVAR design requires large diameter buoyancy modules fitted to the transitional region and the lower region of the riser length. Buoyancy modules were in a set of half shells that fit over the clamp. The buoyancy modules were available in two halves of the desired diameter and variable length with Glass Reinforced

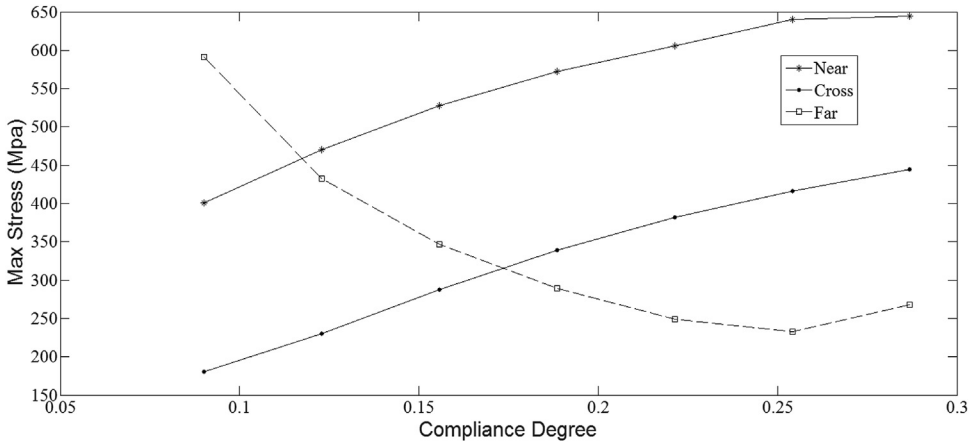

Fig. 7. Impact of compliance on maximum stress.

Epoxy (GRE) skin shell, and filled with epoxy syntactic. The gap was kept between the inside diameter of the buoyancy module and the outside diameter of the insulated riser pipe on which clamps were fitted. Thrust collars were welded to the ends of the riser pipe to eliminate longitudinal movement of the modules. The function of the buoyancy modules was to reduce the payload on the existing TLP.

In the overall analysis of large-scale situations, we studied the factors that influence buoyancy via the concept of a 'buoyancy factor', defined as the buoyancy ratio per unit length versus the unit weight (only the buoyancy factor of transitional region is changed, while the others are constant). Introduction of this concept enabled us to further specify our model parameters.

4.4.1. Buoyancy module location analysis

The pipe section that holds the buoyancy module is 696 m in length. Thus, in order to study the influence of the buoyancy module location, distances were specified between this module and the wellhead of 200 m, 400 m, 600 m, 800 m, and 1,000 m, respectively.

Changes in static configuration and the distribution of effective tension at different distances are shown in Figs. 8 and 9. These results show that although the number of buoyancy modules and the cover section are the same, due to a change of buoyance module location, both static configuration and the effective tension distribution change significantly. The minimum effective tension of the

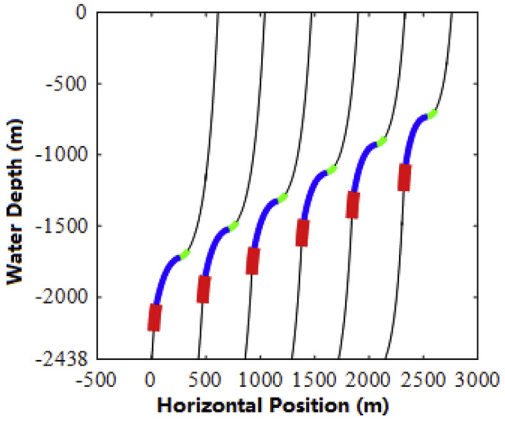

Fig. 8. Static configurations at different buoyancy module locations.

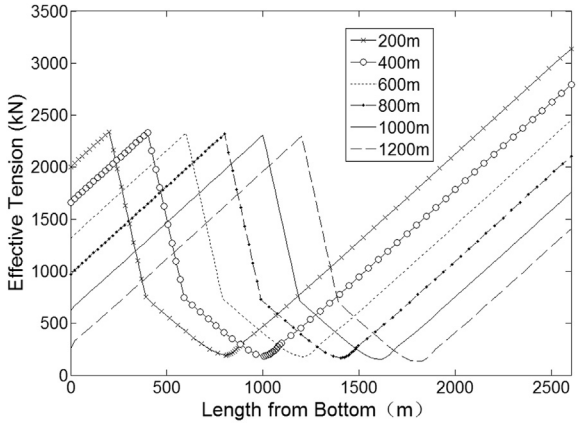

Fig. 9. Effective tension forces at different buoyancy module locations.

whole CVAR is located at the end of transition region, while effective tension at both ends of this transition region are almost unaffected by the location of the buoyancy modules.

However, as the distance from the starting point of the buoyancy block arrangement to the wellhead increases, the top and bottom tension of the riser decrease, and the transition zone of the buoyancy block seems to act as a "separation zone". The tension at the starting point provides a "constant top tension" for the pipe segment below the point, while the tension at the end point provides a "constant bottom tension" for the pipe segment above the point.

The two ends of the CVAR and the transition region are in high stress zones, encompassing two nodes at the ends of the riser and two nodes of maximum stress in the transitional region (Fig. 10). These four nodes are therefore key from the bottom to the top of the CVAR, and are numbered 1, 2, 3, and 4, respectively.

The effect of location of the buoyancy module is shown in Fig. 11; except for node 4, the other three nodes increase in concert with arrangement distance. The stress at node 1 is especially increased because, with the increase of distance between the buoyancy block and the bottom, the insufficient tension results in a large bending stress at the bottom. While node 4 is at the top of the CVAR and the stress comes mainly from the top tension, with the increased distance between the buoyancy module and the bottom, the top tension decreases. For the transition region between node 2 and 3, the stress change is not significant. Thus, the transitional

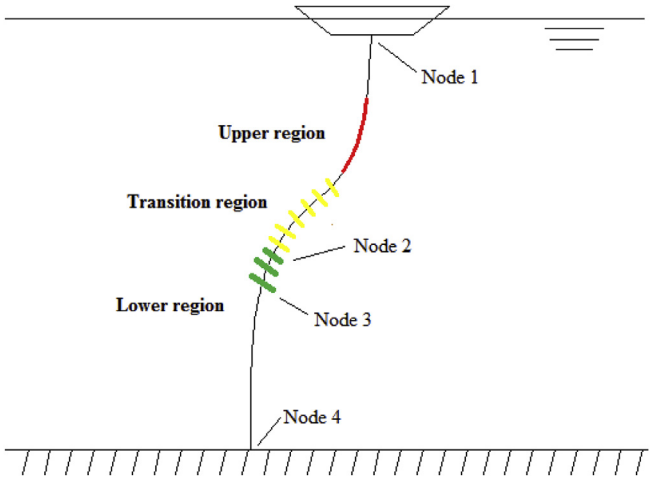

Fig. 10. Four key nodes.

region of the riser should be located near to the wellhead, although not too close, taking into account the need for direct well operation of the well.

4.4.2. Buoyancy factor analysis

The influence of buoyancy factors is shown in Fig. 12, these data show that as buoyancy increases, so does the tension in the lower CVAR region, while that of the upper region is also slowly enhanced. The delivery point in this context appears at the end of the transitional zone, the point where effective tension is smallest.

The influence of buoyancy factors are shown in Fig. 13. These data show that as the buoyancy increases, so does the stress in the lower region and transitional region, while that of the other regions are also slowly enhanced. So, keeping a suitable stress in the lower region and transitional region is the key point when designing buoyancy factors.

Table 3 lists bending moments at critical nodes. These data show that for the bottom of the riser (node 1), the use of both too large and too small buoyancy factors will increase bending moment. An appropriate buoyancy factor can greatly reduce bending moment in this case, for example Cf = 2.2. Data also show that the bending moment at the top of the riser decreases as the buoyancy factor increases; when the buoyancy factor is 1.4, the bending moment at critical nodes remains low. Thus, the CVAR buoyancy factor of bending moment is also significant, and a suitable value should be incorporated into design.

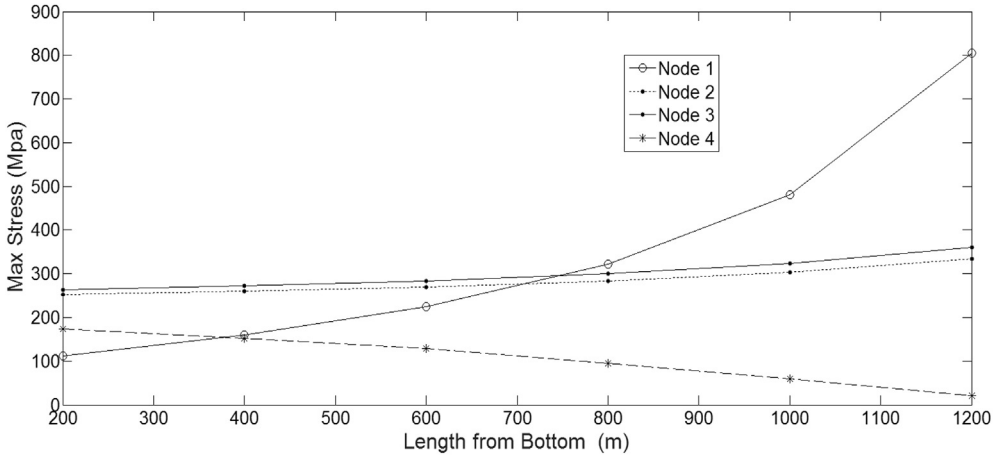

Fig. 11. Key node stresses at different buoyancy module locations.

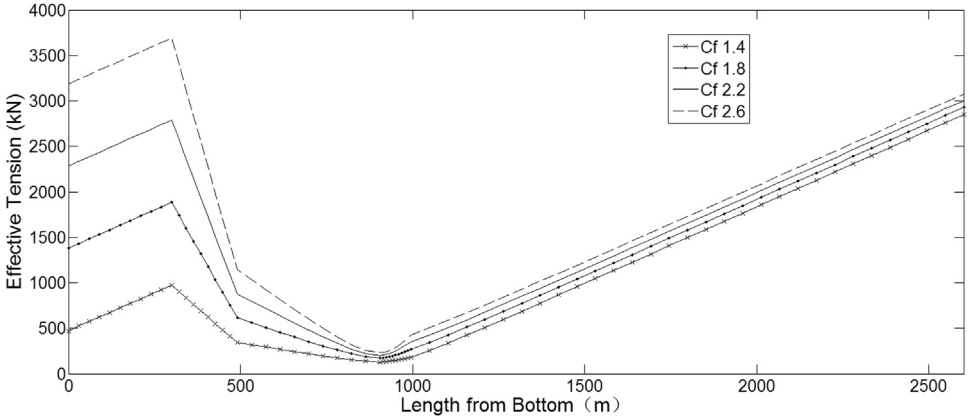

Fig. 12. The impact of buoyancy factors on the effective tension force.

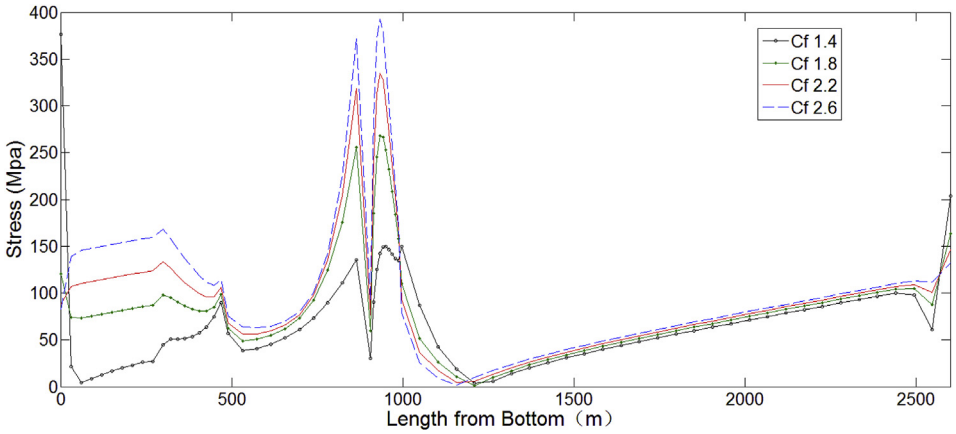

Fig. 13. The impact of buoyancy factors on the stress.

Table 3
The moment of key nodes given different buoyancy factors.

Buoyancy factor (Cf)	Bending moment M/ (kNm)			
	Node 1	Node 2	Node 3	Node 4
1.4	560.2	203.3	245.5	143.5
1.6	295.4	270.6	311.9	114.4
1.8	160.7	331.5	374.4	91.99
2.0	75.5	386.8	430.6	73.13
2.2	15.5	437.3	487.4	56.58
2.4	29.52	483.6	539	41.69
2.6	64.81	526.2	586.9	28.07
2.8	93.35	565.5	631.5	15.47

5. Conclusions

In this paper, based on virtual-work principle and variational principles, a static geometric nonlinear equation of CVARs was derived and the static properties of CVAR were comprehensively analyzed. The results of this study show that the two ends of the riser as well as the transition region are subject to high stress, while the positions of the floating platform exert significant effects on the geometry of the riser configuration. Compliance and buoyancy factor should be set moderately to reduce the CVAR stress. In addition, the buoyancy modules should be placed in the lower region, in order to maximize the operation advantages of CVAR.

Acknowledgements

This research was funded by the National Natural Science Foundation of China (grants 51579245) and the National Key Research and Development Program of China (grant 2016YFC0303800). The authors gratefully acknowledge their financial support.

We thank International Science Editing (http://www.internationalscienceediting.com) for editing this manuscript.

References

Chen, H.F., 2011. Nonlinear Static and Dynamic Analyses of Deepwater Flexible Risers.

Chucheepsakul, S., Monprapussom, T., Huang, T., 2003. Large strain formulations of extensible flexible marine pipes transporting fluid. J. Fluids Struct. 17 (2), 185–224.

Claudio, M.S.Dantas, Marcos, Q.D.Siqueira, Ellwanger, G.B., et al., 2004. A frequency domain approach for random fatigue analysis of steel catenary risers at Brazil's deepwaters. In: ASME 2004 23rd International Conference on Offshore Mechanics and Arctic Engineering, pp. 199–209.

Elosta, H., Huang, S., Incecik, A., 2013. Dynamic response of steel catenary riser using a seabed interaction under random loads. Ocean Eng. 69 (c), 34–43.

Howells, H., 1996. Steel catenary risers west of shetlands. J. Offshore Technol. 4 (2), 6–7.

Kuroiwa, T., Nishigaki, M., 2002. Interaction between riser and tubing in CVAR system. In: Proceedings of the Twelfth International Offshore and Polar Engineering Conference, pp. 26–31.

Martins, C.A., Higashi, E.A., 2000. Parametric analysis of steel catenary risers: fatigue behavior near the top. Proc. Int. Offshore Polar Eng. Conf. 54–59.

Martins, Michele A.L., Lages, Eduardo N., Silveira, Eduardo S.S., 2013. Compliant vertical access riser assessment: DOE analysis and dynamic response optimization. Appl. Ocean Res. 41, 28–40.

Monprapussron, T., Chucheepsakul, S., Huang, T., 2004. The coupled radial-axial deformations analysis of flexible pipes conveying fluid. Int. J. Numer. Methods Eng. 59, 1399–1452.

Mungall, Chris, Haverty, Kevin, Bhat, Shankar, et al., 2004. Semisubmersible based dry tree platform with compliant vertical access risers. In: Offshore Technology Conference, pp. 1–13.

Wang, Y., Duan, M.L., Li, N.N., et al., 2009. Progress of deep water riser installation. Oil Field Equip. 38 (6), 4–8.

Yang, H., Xiao, F., 2014. Instability analyses of a top-tensioned riser under combined vortex and multi-frequency parametric excitations. Ocean Eng. 81 (2), 12–28.

Zhang, X.D., 2002. Calculation method of spatial curve curvature. J. Train Univ. Agric. Reclamation 14 (2), 18–21.

Zhang, C.Z., Wang, G.L., Duan, M.L., et al., 2010. Introduction to the novel hybrid risers in deepwater oil &gas development. Oil Field Equip. 39 (9), 20–25.

Zhen, W.Q., Yang, H.Z., 2010. Dynamic response optimization of a compliant vertical access riser. Ship Sci. Technol. 32 (2), 114–119.